High-Throughput Metabolic Network Analysis and Metatranscriptomics of a Cosmopolitan and Streamlined Freshwater Microbial Lineage

Joshua J. Hamilton[1*], Sarahi L. Garcia^2, Brittany S. Brown^1, Ben O. Oyserman^3, Francisco Moya-Flores^3, Stefan Bertilsson^2,4, Rex R. Malmstrom^5, Katrina T. Forest^1, Katherine D. McMahon^1,3

[1] Department of Bacteriology, University of Wisconsin-Madison, Madison, WI, USA; [2] Department of Ecology and Genetics, Uppsala University, Uppsala, Sweden; [3] Department of Civil and Environmental Engineering, University of Wisconsin-Madison, Madison, WI, USA; [4] Science for Life Laboratory, Uppsala University, Uppsala, Sweden; [5] United States Department of Energy Joint Genome Institute, Walnut Creek, CA, USA

* Correspondence: Joshua J. Hamilton, jjhamilton2@wisc.edu

Abstract

An explosion in the number of available genome sequences obtained through metagenomics and single-cell genomics has enabled a new view of the diversity of microbial life, yet we know surprisingly little about how microbes interact with each other or their environment. In fact, the majority of microbial species remain uncultivated, while our perception of their ecological niches is based on reconstruction of their metabolic potential. In this work, we demonstrate how the “seed set framework”, which computes the set of compounds that an organism must acquire from its environment (Borenstein *et al.*, 2008), enables high-throughput, computational analysis of metabolic reconstructions, while providing new insights into a microbe’s metabolic capabilities, such as nutrient use and auxotrophies. We apply this framework to members of the

ubiquitous freshwater Actinobacterial lineage acI, confirming and extending previous experimental and genomic observations implying that acI bacteria are heterotrophs reliant on peptides and saccharides. We also present the first metatranscriptomic study of the acI lineage, featuring high expression of transport proteins and the light-harvesting protein actinorhodopsin, and confirming predictions of nutrients and essential metabolites while providing additional support to the hypothesis that members of the acI are photoheterotrophs.

Introduction

Natural microbial communities have central roles in the biosphere, ranging from mediators of nutrient cycling to agents of human health and disease (Falkowski *et al.*, 2008; Blaser *et al.*, 2016). However, the majority of microbial species remain uncultivated, a feature that poses a significant challenge to our understanding of their physiology and metabolism. Recent advances in sequencing technology and bioinformatics have enabled assembly and analysis of reference genomes for a wide range of hitherto uncultured community members from diverse environments (Sangwan *et al.*, 2016) that can be explored for inferring links between the genome content of an individual microbe and its metabolic traits, a concept referred to as “reverse ecology” (Levy and Borenstein, 2012).

Reverse ecological analyses can be performed using metabolic network reconstructions (Feist *et al.*, 2009; Thiele and Palsson, 2010), which are structured summaries of the metabolic capabilities of an organism as defined by its enzymes and their coupled biochemical reactions. These reconstructions can then be analyzed using metabolic network graphs, mathematical objects in which biochemical reactions are

represented as connections between substrates and products (Levy and Borenstein, 2012). One such graph-based, reverse ecology approach is to compute an organism's *seed set*, the set of compounds that the organism cannot synthesize on its own and must exogenously acquire from its environment (Borenstein *et al.*, 2008). These compounds may represent both *auxotrophies* for essential metabolites for which biosynthetic routes are missing, and *nutrients* for which degradation but not synthesis routes are present in the genome. This *seed set framework* offers potential advantages over other reconstruction-based approaches, as 1) metabolic network graphs can be rapidly analyzed computationally, 2) a network-centric approach makes no *a priori* assumptions about which metabolic pathways may be important for an organism's niche, and 3) identification of seed compounds facilitates a focused analysis by identifying those compounds that an organism must obtain from its environment.

Freshwater lake microbiomes are ideal systems for applying the seed set framework, as long-term monitoring has revealed the ecology of dominant bacterial lineages (Newton *et al.*, 2011), and reference genomes for these key lineages are now readily available (Martinez-Garcia *et al.*, 2012; Garcia *et al.*, 2013, 2015; Ghai *et al.*, 2014; Ghylin *et al.*, 2014; Tsementzi *et al.*, 2014; Bendall *et al.*, 2016). Among the freshwater bacteria, uncultivated Actinobacteria of the acI lineage are among the most abundant (Zwart *et al.*, 1998, 2002; Glöckner *et al.*, 2000). The acI have been phylogenetically divided into three clades (acI-A, acI-B, and acI-C) and thirteen tribes on the basis of their 16S rRNA gene sequences (Newton *et al.*, 2011). The abundance and ubiquitous distribution of these free-living ultramicrobacteria suggests they have central roles in nutrient cycling in diverse freshwater systems (Glöckner *et al.*, 2000; Newton *et*

al., 2006, 2007; Wu *et al.*, 2006, 2007; De Wever *et al.*, 2008; Humbert *et al.*, 2009; Ghai *et al.*, 2012).

To identify the metabolic processes that these bacteria mediate, the metabolism of the acI lineage has been the focus of a number of recent studies. Surveys using fluorescent *in situ* hybridization (FISH) and catalyzed reporter deposition (CARD) or microautoradiography (MAR) reveal that the acI are capable of consuming amino acids (Salcher *et al.*, 2010, 2013), glucose (Buck *et al.*, 2009; Salcher *et al.*, 2013), N-acetylglucosamine (NAG) (Beier and Bertilsson, 2011; Eckert *et al.*, 2012, 2013), the deoxynucleoside thymidine (Pérez *et al.*, 2010; Salcher *et al.*, 2013), and acetate (Buck *et al.*, 2009). Furthermore, metabolic reconstructions of single-cell genomes (SAGs) and metagenome-assembled genomes (MAGs) have further expanded the view of substrate uptake capabilities for members of clades acI-A and acI-B. These studies indicate members of these clades are capable of consuming a wide array of N-containing compounds, including ammonium, branched-chain amino acids, polyamines, di- and oligo-peptides, and cyanophycin (Ghylin *et al.*, 2014; Garcia *et al.*, 2015). Members of these two clades also seem to be capable of consuming numerous mono-, poly-, and oligo-saccharides (Garcia *et al.*, 2013, 2015; Ghylin *et al.*, 2014). Finally, a recent study of a metagenome-assembled genome from clade acI-B predicted that some members of the clade are unable to synthesize a number of essential vitamins and amino acids (Garcia *et al.*, 2015).

In the present study, we present a computational pipeline to automate the calculation of an organism's substrate utilization capabilities using the seed set framework, thereby facilitating high-throughput analysis of genomic data. To do so, we

92 developed a Python package to predict seed compounds, using metabolic network
93 reconstructions generated from KBase (Arkin *et al.*, 2016). We expand existing
94 analyses of the acI lineage by applying the seed set framework to a reference genome
95 collection of 36 freshwater acI genomes covering all three acI clades. The seed
96 compounds predicted by our analysis are in agreement with previous experimental and
97 genomic observations, confirming the ability of our method to predict an organism's
98 auxotrophies and nutrient sources. To complement these predictions, and to understand
99 which pathways dominate active metabolism of acI in its natural environment, we
100 conducted the first *in situ* metatranscriptomic analysis of gene expression in the acI
101 lineage. Knowledge of seed compounds enhanced interpretation of the
102 metatranscriptome results by facilitating a focused analysis of acI metabolism.
103 Additional analyses show that the acI express a diverse array of transporters that we
104 hypothesize may contribute to their observed dominance and widespread distribution in
105 a variety of aquatic systems.

106 **Materials and Methods**

107 *A Freshwater Reference Genome Collection*

108 This study relies on an extensive collection of freshwater bacterial genomes,
109 containing MAGs obtained from two metagenomic time-series from two Wisconsin lakes
110 (Bendall *et al.*, 2016; Garcia *et al.*, 2016), as well as SAGs from three lakes in the
111 United States (Martinez-Garcia *et al.*, 2012). Additional information about this genome
112 collection can be found in the Supplemental Online Material.

Metatranscriptome Sampling and Sequencing

This study used four metatranscriptomes obtained as part of a 24-hour sampling experiment designed to identify diel trends in freshwater microbial communities. Additional information about these samples can be found in the Supplemental Online Material. All protocols and scripts for sample collection, RNA extraction, rRNA depletion, sequencing, and bioinformatic analysis can be found on Github (https://github.com/McMahonLab/OMD-TOILv2, DOI:######). Metadata for the four samples used in this study can be found in Table S1, and the raw RNA sequences can be found on the National Center for Biotechnology Information (NCBI) website under BioProject PRJNA362825.

Identification of acI SAGs and Actinobacterial MAGs

acI SAGs were identified within a previously-published genome collection (Martinez-Garcia *et al.*, 2012) and classified to the tribe level using partial 16S rRNA genes and a reference taxonomy for freshwater bacteria, as described in the Supplemental Online Material. Actinobacterial MAGs were identified within two metagenomic time-series (Bendall *et al.*, 2016; Garcia *et al.*, 2016) using taxonomic assignments from a subset of conserved marker genes, as described in the Supplemental Online Material. Phylogenetic analysis of acI SAGs and Actinobacterial MAGs was performed using a concatenated alignment of single-copy marker genes obtained via Phylosift (Darling *et al.*, 2014). Maximum likelihood trees were generated using RAxML (Stamatakis, 2014) using the automatic protein model assignment option (PROTGAMMAAUTO) and 100 bootstraps.

Genome Annotation, Metabolic Network Reconstruction, and Computation and Evaluation of Seed Compounds

In the seed set framework, an organism's metabolism is represented via a metabolic network graph, in which nodes denote compounds and edges denote enzymatically-encoded biochemical reactions linking substrates and products (Jeong *et al.*, 2000). Allowable biochemical transformations can be identified by drawing paths along the network, in which a sequence of edges connects a sequence of distinct vertices. In our implementation of the seed set framework, metabolic network graphs were generated as follows.

Genome annotations were performed and metabolic network reconstructions were built using KBase. Contigs for each genome were uploaded to KBase and annotated using the "Annotate Microbial Contigs" method with default options, which uses components of the RAST toolkit for genome annotation (Brettin *et al.*, 2015; Overbeek *et al.*, 2014). Metabolic network reconstructions were obtained using the "Build Metabolic Model" app with default parameters, which relies on the Model SEED framework (Henry *et al.*, 2010) to build a draft metabolic model. These reconstructions were then pruned (currency metabolites and highly-connected compounds) and converted to metabolic network graphs (Figure S1 and Supplemental Online Material). Many of the individual acI genomes are incomplete (see Results). Therefore, composite metabolic network graphs were constructed for each tribe and clade, to increase the accuracy of seed identification by means of a more complete metabolic network (Figure S2 and Supplemental Online Material).

Formally, the seed set of the network is defined as the minimal set of compounds that cannot be synthesized from other compounds in the network, and whose presence enables the synthesis of all other compounds in the network (Borenstein *et al.*, 2008). Seed compounds for each composite metabolic network graph were calculated using a new Python implementation of the seed set framework (Borenstein *et al.*, 2008) (Figure S3 and the Supplemental Online Material). Because seed compounds are computed from a metabolic network, it is important to manually evaluate all predicted seed compounds to identify those that may be biologically meaningful, and do not arise from errors in the metabolic network reconstruction. Examples of this process are given in the Supplemental Online Material.

All computational steps were implemented using Python scripts, freely available as part of the reverseEcology Python package developed for this project (https://pypi.python.org/pypi/reverseEcology/, DOI:######).

Identification of Transported Compounds

For each genome, we identified all transport reactions present in its metabolic network reconstruction. Gene-protein-reaction associations (GPRs) for these reactions were manually curated to remove unannotated proteins, group genes into operons (if applicable), and to identify missing subunits for multi-subunit transporters. These genes were then mapped to their corresponding COGs, and grouped accordingly. Finally, the most common annotation for each COG was used to identify likely substrates for each of these groups.

Protein Clustering, Metatranscriptomic Mapping, and Clade-Level Gene Expression

OrthoMCL (Li *et al.*, 2003) was used to identify clusters of orthologous groups (COGs) in the set of acI genomes. Both OrthoMCL and BLAST were run using default options (Fischer *et al.*, 2011). Annotations were assigned to protein clusters by choosing the most common annotation among all genes assigned to the respective cluster. Trimmed and merged metatranscriptomic reads from each of the four biological samples were then mapped to a single reference fasta file containing all acI genomes using BBMap (https://sourceforge.net/projects/bbmap/) with the *ambig=random* and *minid=0.95* options. The 95% identity cutoff was chosen as this represents a well-established criterion for identifying microbial species using average nucleotide identity (ANI) (Konstantinidis and Tiedje, 2005), while combining the *ambig* option with competitive mapping using pooled acI genomes as the reference ensures that reads map only to a single genome. These results were then used to compute the expression of each COG in each clade.

Next, HTSeq-Count (Anders *et al.*, 2014) was used to count the total number of reads that map to each gene in our acI genome collection. After mapping, the list of counts was filtered to remove those genes that did not recruit at least one read in all four samples. Using the COGs identified by OrthoMCL, the genes that correspond to each COG were then identified.

Within each clade, gene expression for each COG was computed on a Reads Per Kilobase Million (RPKM) basis (Mortazavi *et al.*, 2008), while also accounting for different gene lengths within a COG and numbers of mapped reads for each genome within a clade. That is, the RPKM value for a single COG represents the sum of RPKM

values for each gene within that COG, normalized to the appropriate gene length and total number of mapped reads. RPKM counts were then averaged across the four metatranscriptomes and normalized to the median level of gene expression within that clade.

Availability of Data and Materials

All genomic and metatranscriptomic sequences are available through IMG and NCBI, respectively. A reproducible version of this manuscript is available at https://github.com/joshamilton/Hamilton_acI_2016 (DOI:######).

Results

Phylogenetic Affiliation of acI Genomes

From a reference collection of freshwater bacterial genomes, we identified 17 SAGs and 19 MAGs from members of the acI lineage. A phylogenetic tree of these genomes is shown in Figure 1. Previous phylogenetic analysis using 16S rRNA gene sequences have revealed that the acI lineage can be grouped into three distinct monophyletic clades (Newton *et al.*, 2011). In this study, the phylogenetic tree built from 37 concatenated marker genes also identified three monophyletic branches, enabling MAGs to be classified as clade acI-A or acI-B based on the taxonomy of SAGs within each branch. Note that three MAGs formed a monophyletic group separate from clades acI-A and acI-B; we assume these genomes belong to clade acI-C as no other acI clades have been identified to date.

Estimated Completeness of Tribe- and Clade-Level Composite Genomes

Metabolic network reconstructions created from acI SAGs and MAGs will likely be missing reactions, as the underlying genomes are incomplete (Table 1). Previous studies have examined the effect of genome incompleteness on the predicted seed set (Borenstein *et al.*, 2008). Using the formal (mathematical) definition of a seed compound, this showed that the percentage of correct seed compounds (true positives) is approximately equal to the completeness of the reaction network, and the number of false positives is approximately equal to the incompleteness of the network. Thus, we constructed composite genomes at higher taxonomic levels (e.g., tribe and clade) to increase genome completeness for more accurate seed identification at that taxonomic level.

Using 204 conserved single-copy marker genes (Parks *et al.*, 2015), we estimated the completeness of tribe- and clade-level composite genomes to determine the finest level of taxonomic resolution at which we could confidently compute seed compounds, using genome completeness as a proxy for metabolic reaction network completeness (Figure 2). Because CheckM relies on lineage-specific marker genes, the completeness of genomes without representation in the CheckM database can be underestimated (Garcia *et al.*, 2015). As a result, we deemed genomes to be complete if they contained 95% of the lineage-specific marker genes. With the exception of tribe acI-B1, tribe-level composite genomes are estimated to be incomplete (Figure 2A). At the clade level, clades acI-A and acI-B are estimated to be complete, while the acI-C composite genome remains incomplete, as it only contains 75% of the 204 marker genes (Figure 2B). As a result, seed compounds were calculated for composite clade-

level genomes, with the understanding that some true seed compounds for the acI-C clade will not be predicted.

Computation and Evaluation of Potential Seed Compounds

Seed compounds were computed for each clade, using the composite metabolic network graph for that clade (Figure 3, and Figures S1 to S3). A total of 125 unique seed compounds were identified across the three clades (Table S2). Additional details are available in the Supplemental Online Material.

Seed compounds were predicted using the results of an automated annotation pipeline, and as such are likely to contain inaccuracies (e.g., due to missing or incorrect annotations). As a result, we screened the set of predicted seed compounds to identify those that represented biologically plausible auxotrophies and nutrients, and manually curated this subset to obtain a final set of auxotrophies and nutrient sources. Compounds involved in fatty acid and phospholipid biosynthesis pathways were removed during curation, as these pathways are often organism-specific and unlikely to be properly annotated by automatic metabolic reconstruction pipelines. Seed compounds related to currency metabolites were also removed, as reactions for the synthesis of these compounds may have been removed during network pruning. Of 125 unique compounds, 39 (31%) passed this screening and were deemed biologically plausible.

The Supplemental Online Material contains a series of brief vignettes explaining why select compounds were discarded based on the afore-mentioned considerations, and provides examples of additional curation efforts applied to biologically plausible compounds. For a plausible auxotrophy, we screened the genomes for the canonical

biosynthetic pathway(s) for that compound, and retained those compounds for which the biosynthetic pathway was incomplete. For a plausible nutrient source, we screened the genomes for the canonical degradation pathway(s) for that compound, and retained those compounds for which the degradation pathway was complete. Of the 39 compounds deemed biologically plausible auxotrophies and nutrients, 31 (79%) were retained in the final set of proposed auxotrophies and nutrients. Tables S6 and S7 contain this final set of compounds for clades acI-A, acI-B, and acI-C, and Figure 4 shows the auxotrophies and nutrients these compounds represent.

Making Sense of Seed Compounds via Protein Clustering and Metatranscriptomic Mapping

With regards to seed compounds representing nutrient sources, genes associated with the consumption of these compounds should be expressed. However, because seed compounds were computed from each clade's composite metabolic network graph, genes associated with the consumption of seed compounds may be present in multiple genomes within the clade. To facilitate the linkage of metatranscriptome measurements to seed compounds, we decided to map metatranscriptome samples to clusters of orthologous groups (COGs) within each clade. We used OrthoMCL (Li *et al.*, 2003) to identify COGs in the set of acI genomes, and counted each COG as present in a clade if that COG was present in at least one genome belonging to that clade. We then used BBMap to map metatranscriptome reads to our reference genome collection, and counted the unique reads which map to each Actinobacterial COG.

Sequencing of cDNA from all four rRNA-depleted metatranscriptome samples yielded approximately 160 billion paired-end reads. After merging, filtering, and further *in-silico* rRNA removal, approximately 81 billion, or 51% of the reads remained (Table S1). OrthoMCL identified a total of 5013 protein clusters across the three clades (Table S3). The COGs were unequally distributed across the three clades, with clade acI-A genomes containing 3175 COGs (63%), clade acI-B genomes containing 3459 COGs (69%), and clade acI-C genomes containing 1365 COGs (27%). After mapping the metatranscriptomes to our acI genomes (Table S4), we identified 650 COGs expressed in clade acI-A, 785 in clade acI-B, and 849 in clade acI-C (Table S5). Among expressed genes, the median log2 average RPKM value was 10.3 in clade acI-A, 10.2 in clade acI-B, and 9.0 in clade acI-C. Thus, despite differential abundance of each clade within the lake, median gene expression within each clade was similar.

Auxotrophies and Nutrient Sources of the acI Lineage

Seed set analysis yielded seven auxotrophies that could be readily mapped to ecophysiological attributes of the acI lineage (Figure 4a). In all three clades, beta-alanine was identified as a seed compound, suggesting an auxotrophy for pantothenic acid (Vitamin B5), a precursor to coenzyme A formed from beta-alanine and pantoate. In bacteria, beta-alanine is typically synthesized via aspartate decarboxylation, and we were unable to identify a candidate gene for this enzyme (aspartate 1-decarboxylase, E.C. 4.1.1.11) in any acI genome. Pyridoxine 5'-phosphate and 5'-pyridoxamine phosphate (forms of the enzyme cofactor pyridoxal 5'-phosphate, Vitamin B6) were also predicted to be seed compounds, and numerous enzymes in the biosynthesis of these compounds were not found in the genomes.

Clades within the acI lineage also exhibited distinct auxotrophies. Clade acI-A was predicted to be auxotrophic for the cofactor tetrahydrofolate (THF or Vitamin B9), and numerous enzymes for its biosynthesis were missing. This cofactor plays an important role in the metabolism of amino acids and vitamins. In turn, clade acI-B was predicted to be auxotrophic for adenosylcobalamin (Vitamin B12), containing only a single reaction from its biosynthetic pathway. Finally, acI-C was predicted to be auxotrophic for the nucleotide uridine monophosphate (UMP, used as a monomer in RNA synthesis) and the amino acids lysine and homoserine. In all cases multiple enzymes for the biosynthesis of these compounds were not found in the acI-C genomes. However, with the exception of adenosylcobalamin, we did not identify transporters for any of these compounds. Furthermore, because the acI-C composite genome was estimated to be around 75% complete, we cannot rule out the possibility that the missing genes might be found in when additional genomes are recovered.

A number of seed compounds were predicted to be nutrients, compounds which can be degraded by members of the acI lineage (Figure 4B). Both clades acI-A and acI-B were predicted to use D-altronate and trans-4-hydroxy proline as nutrients, and acI-B was additionally predicted to use glycine betaine. These compounds indicate that the acI may participate in the turnover of plant- and animal-derived organic material in freshwater systems: glycine betaine is an important osmolyte in plants (Ashraf and Foolad, 2007), D-altronate is produced during degradation of galacturonate, a component of plant pectin (Mohnen, 2008), and trans-4-hydroxy-L-proline is a major component of animal collagen (Eastoe, 1955).

Finally, all three clades were predicted to use di-peptides and the sugar maltose as nutrients. Clades acI-A and acI-C were also predicted to consume the polysaccharides stachyose, manninotriose, and cellobiose. In all cases, these compounds were associated with reactions catalyzed by peptidases or glycoside hydrolases (Table S8 and S9), which may be capable of acting on compounds beyond the predicted seed compounds. Thus, we used these annotations to define nutrient sources, rather than using the predicted seed compounds themselves. Among these nutrient sources were di- and polypeptides, predicted to be released from both cytosolic- and membrane-bound aminopeptidases. As discussed below, we identified a number of transport proteins capable of transporting these released residues. In Lake Mendota, these aminopeptidases were expressed in clades acI-A and acI-B at around 70% of the median gene expression levels, while they were expressed at up to twice the median in clade acI-C (Table S8). These findings agrees with MAR-FISH and CARD-FISH studies that confirm the ability of acI bacteria to consume a variety of amino acids (Salcher *et al.*, 2010, 2013).

All three clades were predicted to encode an alpha-glucosidase, which in Lake Mendota was expressed most strongly in clade acI-C, at approximately 116% of the median (Table S9). Clades acI-A and acI-C also encode a beta-glucosidase, but it was not expressed, at least under prevailing environmental conditions. Both of these enzymes release glucose monomers, which acI is known to consume (Buck *et al.*, 2009; Salcher *et al.*, 2013). Furthermore, these two clades encode an alpha-galactosidase and multiple maltodextrin glucosidases (which free maltose from maltotriose), but these were only expressed in clade acI-C during our sampling period. The alpha-

357 galactosidase had a log2 average RPKM expression value of 2.5 times the median,
358 while the maltodextrin glucosidases were expressed at approximately 20% of the
359 median (Table S9).

360 *Compounds Transported by the acI Lineage*

361 Microbes may be capable of transporting compounds that are not strictly required
362 for growth, and comparing such compounds to predicted seed compounds can provide
363 additional information about an organism's ecology. Thus, we used the metabolic
364 network reconstructions for the acI genomes to systematically characterize the transport
365 capabilities of the acI lineage.

366 All acI clades encode for and expressed a diverse array of transporters (Figure 5,
367 Tables S10 and S11, and the Supplemental Online Material). Consistent with the
368 presence of peptidases, all clades contain numerous genes for the transport of peptides
369 and amino acids, including multiple oligopeptide and branched-chain amino acid
370 transporters, as well as two distinct transporters for the polyamines spermidine and
371 putrescine. All clades also contain a transporter for ammonium. As averaged over the
372 24-hour sampling period, the ammonium, branched-chain amino acid, and oligopeptide
373 transporters had expression values above the median, with expression values for the
374 substrate-binding protein (of the ATP-binding cassette (ABC) transporters) ranging from
375 2 to 325 times the median (Table S10). In contrast, while all clades expressed some
376 genes from the polyamine transporters, only clade acI-B expressed the
377 spermidime/putrescine binding protein, at approximately 75 times the median (Table
378 S10). Additionally, clade acI-A contains a third distinct branched-chain amino acid
379 transporter, composed of COGs not found in clades acI-B or acI-C. This transporter was

not as highly expressed as the shared transporters, with the substrate-binding protein not expressed at all (Table S10). Finally, clades acI-A and acI-B also contain a transporter for glycine betaine, which was only expressed in clade acI-A, at approximately 35 times the median (Table S10). However, because these observations were made at a single site at a single point in time, we cannot rule out the possibility that the expression of these transporters changes with space and time.

All clades also strongly expressed transporters consistent with the presence of glycoside hydrolases, including transporters for the sugars maltose (a dimer of glucose) and xylose, with expression values for the substrate-binding protein ranging from 3 to 144 times the median (Table S10). Clades acI-A and acI-B also contain four distinct transporters for ribose, although the substrate-binding subunit was not expressed at the time of sampling (Table S10).

Representatives from the acI lineage also encode and expressed a number of transporters that do not have corresponding seed compounds, including a uracil permease, and a xanthine/uracil/thiamine/ascorbate family permease, both of which are expressed at levels ranging from 11 to 127 times the median (Table S10) during the sampling period. Clades acI-A and acI-B also contain a cytosine/purine/uracil/thiamine/allantoin family permease, even if it was only expressed in clade acI-B at the time of sampling (Table S10). Though not strictly annotated as such, all three of these transporters may be responsible for the uptake of the seed compound UMP. In addition, clade acI-A contains but did not express a transporter for cobalamin (Vitamin B12), and both clades acI-A and acI-B contain but did not express transporters for thiamin (Vitamin B1) and biotin (Vitamin B7) (Table S10). Despite

403 predicted auxotrophies for Vitamins B5 and B6, we were unable to find transporters for
404 these two compounds. However, as identification and annotation of transport proteins is
405 an active area of research (Saier *et al.*, 2014), transporters for these vitamins may yet
406 be present in the genomes.

407 Finally, all three clades expressed actinorhodopsin, a light-sensitive protein that
408 functions as an proton efflux pump (Sharma *et al.*, 2008). In all clades, actinorhodopsin
409 was among the top seven most highly-expressed genes at the time of sampling (Table
410 S4), with expression values in excess of 300 times the median in all three clades (Table
411 S4). Given that many of the transport proteins are ABC transporters, we speculate that
412 actinorhodopsin may facilitate maintenance of the proton gradient necessary for ATP
413 synthesis. Above-median expression of the ATP synthase genes is consistent with this
414 hypothesis. Coupled with high expression levels of diverse transporters, this result
415 strongly suggests that acI functioned as a photoheterotroph and was actively pumping
416 protons during our sampling period. However, it remains to be seen if this behavior is a
417 general feature of acI ecology or restricted to the specific conditions of the lake and our
418 sampling period.

419 **Discussion**

420 This study introduces the use of high-throughput metabolic network
421 reconstruction and the seed set framework to predict auxotrophies and nutrient sources
422 of uncultivated microorganisms from incomplete genome sequences. By leveraging
423 multiple genomes from closely related populations, we were able to construct composite
424 genomes for individual acI clades. Obviously this masks differences among tribes as
425 well as smaller populations and individual cells, and may sometimes overestimate the

426 metabolic capabilities of a clade or group. However, it provides a framework that can be
427 used to generate new hypotheses about the substrates used by members of a defined
428 phylogenetic group, provided multiple closely related genomes are available. As
429 metagenomic assembly and binning techniques and single cell sequencing methods
430 improve and complete genomes become available, we anticipate our approach being
431 applied to individual microbial genomes.

432 Our predictions of substrate use capabilities of the acI lineage are largely
433 congruent with previous genome-based studies based on smaller but manually curated
434 genome collections, indicating that the use of automatic metabolic network
435 reconstructions yields similar predictions to manual metabolic reconstruction efforts,
436 while being both high-throughput and focused on an organism's substrate utilization
437 capabilities. In particular, this study predicts that the consumption of N-rich compounds
438 is a universal feature of the acI lineage, with all three clades predicted to consume
439 ammonium, branched-chain amino acids, and di- and oligopeptides. We provide new
440 evidence for further specialization within each clade, identifying unique substate binding
441 proteins for some of their amino acid and peptide transporters (see Supplemental
442 Online Material), and the expression of a transporter for the polyamines spermidine and
443 putrescine in clade acI-B. Furthermore, we confirm the ability of all three clades to
444 consume xylose and maltose, and of clades acI-A and acI-B to consume ribose.
445 However, despite the presence and expression of alpha-glucosidases in all three
446 clades, and beta-glucosidases in clades acI-A and acI-B, no obvious glucose transport
447 system was found in the genomes. Our analysis also made novel predictions, including

448 the presence of beta-glucosidases, as well as alpha- and beta-galactosidases, in clades
449 acI-A and acI-C.

450 This study also suggests that auxotrophies for some vitamins may be universal
451 features of the acI lineage, as we predict all clades to be auxotrophic for pantothenic
452 acid and pyridoxal 5'-phosphate (Vitamins B5 and B6). We also predict new
453 auxotrophies within the acI lineage, including THF (clade acI-A), and lysine,
454 homoserine, and UMP (clade acI-C). While our acI-C composite genome remains
455 incomplete, these results nonetheless provide additional support to the hypothesis that
456 distributed metabolic pathways and metabolic complementarity may be common
457 features of freshwater bacterial communities (Garcia *et al.*, 2015; Garcia, 2016).

458 Combined, these results indicate that acI are photoheterotrophs, making a living
459 on a diverse array of N-rich compounds, sugars, oligo- and poly-saccharides, and light.
460 We hypothesize that the acI obtain peptides from the products of cell lysis, and may
461 participate in the turnover of high molecular weight dissolved organic compounds, such
462 as starch, glycogen, and cellulose. The acI lineage does not appear to be metabolically
463 self-sufficient, relying on other organisms for the production of essential nutrients.

464 This study also presents the first combined genomic and metatranscriptomic
465 analysis of a freshwater microbial lineage. Transport proteins were among the most
466 highly expressed in the acI genomes, and the expression of multiple amino acid
467 transporters may facilitate uptake of these labile compounds. We also observed
468 differences in the relative expression of these transporters, which may point to clade-
469 specific differences in the affinity for these substrates. Finally, the actinorhodopsin

protein was highly expressed, and may facilitate synthesis of the ATP needed to drive acI's many ABC-type transporters.

A close comparison of our predictions to previous studies of the acI lineage reveals some important limitations of the seed set framework and automatic metabolic reconstructions. First, the seed set framework only identifies compounds that the metabolic network **must** obtain from its environment, and will fail to identify compounds that the organism can acquire from its environment but can also synthesize itself. For example, members of clades acI-A and acI-B are capable of consuming branched-chain amino acids (Ghylin *et al.*, 2014; Garcia *et al.*, 2015), but can also synthesize them. Thus, these compounds were not identified as seed compounds. However, transport reactions for branched-chain amino acids were identified in the genomes, and our metatranscriptomic found them to be highly expressed.

Second, automatic metabolic network reconstructions may not fully capture an organism's metabolic network (e.g., due to missing or incorrect genome annotations). For example, previous genome-based studies have suggested that members of the acI lineage harbor cyanophycinase, an enzyme that allows them to hydrolyze the cyanobacterial peptide cyanophycin (Garcia *et al.*, 2013; Ghylin *et al.*, 2014). Manual inspection revealed that KBase annotated this putative enzyme as a hypothetical protein, and we could not identify transporters for cyanophycin in the metabolic network reconstruction. As biochemical characterization of hypothetical proteins and automatic gene and protein annotation are active areas of research, we anticipate that advances in these fields will continue to improve the accuracy of automatic metabolic network reconstructions.

Conclusions

In this study, we examined the ecological niche of uncultivated acI bacteria using automatic metabolic network reconstructions and the seed set framework combined with metatranscriptomics. Predicted seed compounds include peptides and saccharides, many of which acI have been observed to consume *in situ*, as well as newly predicted auxotrophies for vitamins and amino acids. Metatranscriptomic analysis in a lake with abundant acI members suggests many of these compounds are consumed by acI bacteria in their natural environment. Our high-throughput approach easily scales to 100s of genomes, and enables a focused metabolic analysis by identifying those compounds through which an organism interacts with its environment. Finally, the seed set framework enables additional reverse ecological analyses, which promise to predict the interactions among microbial species in complex environments (Levy and Borenstein, 2012).

Acknowledgements

We thank past members of the McMahon lab for collecting water samples for single-cell sequencing and metagenomic sequencing. This work was supported through the JGI Community Science Program. The work conducted by the JGI, a DOE Office of Science User Facility, is supported by the Office of Science of the U.S. Department of Energy under Contract No. DE-AC02-05CH11231. This material is based upon work that is supported by the National Institute of Food and Agriculture, U.S. Department of Agriculture, under award number 2016-67012-24709 to JJH and WIS01789 to KDM. KDM also acknowledges funding from the United States National Science Foundation (NSF) Microbial Observatories program (MCB-0702395), the NSF Long Term

Ecological Research program (NTL-LTER DEB-1440297), an NSF INSPIRE award (DEB-1344254), and the University of Wisconsin System. KDM and KTF acknowledge National Oceanic and Atmospheric Administration (NOAA) grant #NA10OAR4170070, Wisconsin Sea Grant College Program Project #HCE-25, through NOAA'S National Sea Grant College Program, U.S. Department of Commerce.

Conflict of Interest

The authors declare no conflict of interest.

References

Anders S, Pyl PT, Huber W. (2014). HTSeq A Python framework to work with high-throughput sequencing data. *Bioinformatics* **31**: 166–169.

Arkin AP, Stevens RL, Cottingham RW, Maslov S, Henry CS, Dehal P *et al.* (2016). The DOE Systems Biology Knowledgebase (KBase). *bioRxiv*. e-pub ahead of print, doi: 10.1101/096354.

Ashraf M, Foolad MR. (2007). Roles of glycine betaine and proline in improving plant abiotic stress resistance. *Environmental and Experimental Botany* **59**: 206–216.

Beier S, Bertilsson S. (2011). Uncoupling of chitinase activity and uptake of hydrolysis products in freshwater bacterioplankton. *Limnology and Oceanography* **56**: 1179–1188.

Bendall ML, Stevens SLR, Chan L-K, Malfatti S, Schwientek P, Tremblay J *et al.* (2016). Genome-wide selective sweeps and gene-specific sweeps in natural bacterial populations. *The ISME Journal* **10**: 1589–1601.

537 Blaser MJ, Cardon ZG, Cho MK, Dangl JL, Donohue TJ, Green JL *et al.* (2016). Toward
538 a Predictive Understanding of Earth's Microbiomes to Address 21st Century
539 Challenges. *mBio* **7**: e00074–16.
540 Borenstein E, Kupiec M, Feldman MW, Ruppin E. (2008). Large-scale reconstruction
541 and phylogenetic analysis of metabolic environments. *Proceedings of the*
542 *National Academy of Sciences* **105**: 14482–14487.
543 Brettin T, Davis JJ, Disz T, Edwards RA, Gerdes S, Olsen GJ *et al.* (2015). RASTtk: a
544 modular and extensible implementation of the RAST algorithm for building
545 custom annotation pipelines and annotating batches of genomes. *Scientific*
546 *Reports* **5**: 8365.
547 Buck U, Grossart H-P, Amann RI, Pernthaler J. (2009). Substrate incorporation patterns
548 of bacterioplankton populations in stratified and mixed waters of a humic lake.
549 *Environmental Microbiology* **11**: 1854–1865.
550 Darling AE, Jospin G, Lowe E, Matsen FA, Bik HM, Eisen JA. (2014). PhyloSift:
551 phylogenetic analysis of genomes and metagenomes. *PeerJ* **2**: e243.
552 De Wever A, Van Der Gucht K, Muylaert K, Cousin S, Vyverman W. (2008). Clone
553 library analysis reveals an unusual composition and strong habitat partitioning of
554 pelagic bacterial communities in Lake Tanganyika. *Aquatic Microbial Ecology* **50**:
555 113–122.
556 Eastoe JE. (1955). The amino acid composition of mammalian collagen and gelatin.
557 *The Biochemical Journal* **61**: 589–600.

558 Eckert EM, Baumgartner M, Huber IM, Pernthaler J. (2013). Grazing resistant
559 freshwater bacteria profit from chitin and cell-wall-derived organic carbon.
560 *Environmental Microbiology* **15**: 2019–2030.
561 Eckert EM, Salcher MM, Posch T, Eugster B, Pernthaler J. (2012). Rapid successions
562 affect microbial N-acetyl-glucosamine uptake patterns during a lacustrine spring
563 phytoplankton bloom. *Environmental Microbiology* **14**: 794–806.
564 Falkowski PG, Fenchel T, Delong EF. (2008). The microbial engines that drive Earth's
565 biogeochemical cycles. *Science* **320**: 1034–1039.
566 Feist AM, Herrgård MJ, Thiele I, Reed JL, Palsson BØ. (2009). Reconstruction of
567 biochemical networks in microorganisms. *Nature Reviews Microbiology* **7**: 129–
568 143.
569 Fischer S, Brunk BP, Chen F, Gao X, Harb OS, Iodice JB *et al.* (2011). Using OrthoMCL
570 to assign proteins to OrthoMCL-DB groups or to cluster proteomes into new
571 ortholog groups. *Current Protocols in Bioinformatics* **Supplement**: 6.12.1.6–
572 12.19.
573 Gao B, Gupta RS. (2012). Phylogenetic Framework and Molecular Signatures for the
574 Main Clades of the Phylum Actinobacteria. *Microbiology and Molecular Biology*
575 *Reviews* **76**: 66–112.
576 Garcia SL. (2016). Mixed cultures as model communities: hunting for ubiquitous
577 microorganisms, their partners, and interactions. *Aquatic Microbial Ecology* **77**:
578 79–85.

579 Garcia SL, Buck M, McMahon KD, Grossart H-P, Eiler A, Warnecke F. (2015).
580 Auxotrophy and intra-population complementary in the 'interactome' of a
581 cultivated freshwater model community. *Molecular Ecology* **24**: 4449–4459.
582 Garcia SL, McMahon KD, Martinez-Garcia M, Srivastava A, Sczyrba A, Stepanauskas
583 R *et al.* (2013). Metabolic potential of a single cell belonging to one of the most
584 abundant lineages in freshwater bacterioplankton. *The ISME Journal* **7**: 137–147.
585 Garcia SL, Stevens SLR, Crary B, Martinez-Garcia M, Stepanauskas R, Woyke T *et al.*
586 (2016). Contrasting patterns of genome-level diversity across distinct co-
587 occurring bacterial populations. *bioRxiv*. e-pub ahead of print, doi:
588 http://dx.doi.org/10.1101/080168.
589 Ghai R, McMahon KD, Rodriguez-Valera F. (2012). Breaking a paradigm: cosmopolitan
590 and abundant freshwater actinobacteria are low GC. *Environmental Microbiology*
591 *Reports* **4**: 29–35.
592 Ghai R, Mizuno CM, Picazo A, Camacho A, Rodriguez-Valera F. (2014). Key roles for
593 freshwater Actinobacteria revealed by deep metagenomic sequencing. *Molecular*
594 *Ecology* **23**: 6073–6090.
595 Ghylin TW, Garcia SL, Moya F, Oyserman BO, Schwientek P, Forest KT *et al.* (2014).
596 Comparative single-cell genomics reveals potential ecological niches for the
597 freshwater acI Actinobacteria lineage. *The ISME Journal* **8**: 2503–2516.
598 Glöckner FO, Zaichikov E, Belkova N, Denissova L, Pernthaler J, Pernthaler A *et al.*
599 (2000). Comparative 16S rRNA analysis of lake bacterioplankton reveals globally
600 distributed phylogenetic clusters including an abundant group of actinobacteria.
601 *Applied and Environmental Microbiology* **66**: 5053–5065.

602 Henry CS, DeJongh M, Best AA, Frybarger PM, Linsay B, Stevens RL. (2010). High-
603 throughput generation, optimization and analysis of genome-scale metabolic
604 models. *Nature Biotechnology* **28**: 977–982.
605 Humbert JF, Dorigo U, Cecchi P, Le Berre B, Debroas D, Bouvy M. (2009). Comparison
606 of the structure and composition of bacterial communities from temperate and
607 tropical freshwater ecosystems. *Environmental Microbiology* **11**: 2339–2350.
608 Jeong H, Tombor B, Albert R, Oltvai ZN, Barabási A-L, Database I. (2000). The large-
609 scale organization of metabolic networks. *Nature* **407**: 651–654.
610 Konstantinidis KT, Tiedje JM. (2005). Genomic insights that advance the species
611 definition for prokaryotes. *Proceedings of the National Academy of Sciences* **102**:
612 2567–2572.
613 Levy R, Borenstein E. (2012). Reverse Ecology: From Systems to Environments and
614 Back. Soyer OS (ed). *Advances in Experimental Medicine and Biology* **751**: 329–
615 345.
616 Li L, Stoeckert CJ, Roos DS. (2003). OrthoMCL: identification of ortholog groups for
617 eukaryotic genomes. *Genome Research* **13**: 2178–89.
618 Ma H, Zeng A-P. (2003). Reconstruction of metabolic networks from genome data and
619 analysis of their global structure for various organisms. *Bioinformatics* **19**: 270–
620 277.
621 Martinez-Garcia M, Swan BK, Poulton NJ, Gomez ML, Masland D, Sieracki ME *et al.*
622 (2012). High-throughput single-cell sequencing identifies photoheterotrophs and
623 chemoautotrophs in freshwater bacterioplankton. *The ISME Journal* **6**: 113–123.

624 Mohnen D. (2008). Pectin structure and biosynthesis. *Current Opinion in Plant Biology*
625 **11**: 266–277.
626 Mortazavi A, Williams BA, McCue K, Schaeffer L, Wold B. (2008). Mapping and
627 quantifying mammalian transcriptomes by RNA-Seq. *Nature Methods* **5**: 621–
628 628.
629 Newton RJ, Jones SE, Eiler A, McMahon KD, Bertilsson S. (2011). A guide to the
630 natural history of freshwater lake bacteria. *Microbiology and Molecular Biology*
631 *Reviews* **75**: 14–49.
632 Newton RJ, Jones SE, Helmus MR, McMahon KD. (2007). Phylogenetic ecology of the
633 freshwater Actinobacteria acI lineage. *Applied and Environmental Microbiology*
634 **73**: 7169–7176.
635 Newton RJ, Kent AD, Triplett EW, McMahon KD. (2006). Microbial community dynamics
636 in a humic lake: differential persistence of common freshwater phylotypes.
637 *Environmental Microbiology* **8**: 956–970.
638 Overbeek RA, Olson R, Pusch GD, Olsen GJ, Davis JJ, Disz T *et al.* (2014). The SEED
639 and the Rapid Annotation of microbial genomes using Subsystems Technology
640 (RAST). *Nucleic Acids Research* **42**: 206–214.
641 Parks DH, Imelfort M, Skennerton CT, Hugenholtz P, Tyson GW. (2015). CheckM:
642 assessing the quality of microbial genomes recovered from isolates, single cells,
643 and metagenomes. *Genome Research* **25**: 1043–1055.
644 Pérez MT, Hörtnagl P, Sommaruga R. (2010). Contrasting ability to take up leucine and
645 thymidine among freshwater bacterial groups: Implications for bacterial
646 production measurements. *Environmental Microbiology* **12**: 74–82.

647 Saier MH, Reddy VS, Tamang DG, Västermark Å. (2014). The transporter classification
648 database. *Nucleic Acids Research* **42**: D251–D258.
649 Salcher MM, Pernthaler J, Posch T. (2010). Spatiotemporal distribution and activity
650 patterns of bacteria from three phylogenetic groups in an oligomesotrophic lake.
651 *Limnology and Oceanography* **55**: 846–856.
652 Salcher MM, Posch T, Pernthaler J. (2013). In situ substrate preferences of abundant
653 bacterioplankton populations in a prealpine freshwater lake. *The ISME Journal* **7**:
654 896–907.
655 Sangwan N, Xia F, Gilbert JA. (2016). Recovering complete and draft population
656 genomes from metagenome datasets. *Microbiome* **4**: 8.
657 Sharma AK, Zhaxybayeva O, Papke RT, Doolittle WF. (2008). Actinorhodopsins:
658 Proteorhodopsin-like gene sequences found predominantly in non-marine
659 environments. *Environmental Microbiology* **10**: 1039–1056.
660 Stamatakis A. (2014). RAxML version 8: a tool for phylogenetic analysis and post-
661 analysis of large phylogenies. *Bioinformatics* **30**: 1312–1313.
662 Thiele I, Palsson BØ. (2010). A protocol for generating a high-quality genome-scale
663 metabolic reconstruction. *Nature Protocols* **5**: 93–121.
664 Tsementzi D, Poretsky RS, Rodriguez-R LM, Luo C, Konstantinidis KT. (2014).
665 Evaluation of metatranscriptomic protocols and application to the study of
666 freshwater microbial communities. *Environmental Microbiology Reports* **6**: 640–
667 655.
668 Wu QL, Zwart G, Schauer M, Kamst-Van Agterveld MP, Hahn MW. (2006).
669 Bacterioplankton community composition along a salinity gradient of sixteen

high-mountain lakes located on the Tibetan Plateau, China. *Applied and Environmental Microbiology* **72**: 5478–5485.

Wu X, Xi W, Ye W, Yang H. (2007). Bacterial community composition of a shallow hypertrophic freshwater lake in China, revealed by 16S rRNA gene sequences. *FEMS Microbiology Ecology* **61**: 85–96.

Zwart G, Crump BC, Kamst-Van Agterveld MP, Hagen F, Han S-K. (2002). Typical freshwater bacteria: an analysis of available 16S rRNA gene sequences from plankton of lakes and rivers. *Aquatic Microbial Ecology* **28**: 141–155.

Zwart G, Hiorns WD, Methé BA, Agterveld MP van, Huismans R, Nold SC *et al.* (1998). Nearly identical 16S rRNA sequences recovered from lakes in North America and Europe indicate the existence of clades of globally distributed freshwater bacteria. *Systematic and Applied Microbiology* **21**: 546–556.

683 **Figure Captions**

684 *Figure 1*

685

686 Phylogenetic placement of the genomes used in this study within the acI lineage.
687 The tree was built using RAxML (Stamatakis, 2014) from a concatenated alignment of
688 protein sequences from 37 single-copy marker genes (Darling *et al.*, 2014). The order
689 Actinomycetales forms the outgroup. Vertical black bars indicate groups of genomes
690 belonging to defined tribes/clades within the acI lineage, as determined using 16S rRNA
691 gene sequences (for SAGs and bin FNEF8-2 bin_7 acI-B only) and a defined taxonomy
692 (Newton *et al.*, 2011). SAGs are indicated with italic text. Supplemental Figure S5
693 shows the position of the acI lineage relative to other orders within the class
694 Actinobacteria.

695

696 *Figure 2*

697

698 Mean estimated completeness of tribe-level (clade-level) population genomes as
699 a function of the number of sampled genomes. For each tribe (clade), genomes were
700 randomly sampled (with replacement) from the set of all genomes belonging to that tribe
701 (clade). Completeness was estimated using 204 single-copy marker genes from the
702 phylum Actinobacteria (Parks *et al.*, 2015). Error bars represent the 95% confidence
703 interval estimated from 1000 iterations.

704

Figure 3

Overview of the seed set framework and metatranscriptomic mapping, using three genomes from the acI-C clade as an example. **(A)** Metabolic network graphs are created for each genome belonging to clade acI-C. In these graphs, metabolites are represented as nodes (circles) and reactions by arcs (arrows). Grey nodes and edges indicate components of the composite graph missing from that genome graph. Additional information on this step of the workflow is available in Figure S1. **(B)** A composite network graph is created for each clade by joining graphs for all genomes from that clade, and seed compounds (red) are computed for the composite graph. Additional information on this step of the workflow is available in Figures S2, S3, and S4. **(Inset)** Three seed compounds which indicate an auxotrophy for L-homoserine, a methionine precursor. **(C)** Metatranscriptomic reads are mapped to each individual genome using BBMap. Orthologous gene clusters are identified using OrthoMCL (Li *et al.*, 2003). For each cluster, unique reads which map to any gene within that cluster are counted using HTSeq (Anders *et al.*, 2014). The relative gene expression is computed using RPKM (Mortazavi *et al.*, 2008).

Figure 4

Seed compounds of members of the acI lineage. **(A)** Auxotrophies and nutrient sources, not including peptides and glycosides. **(B)** Peptides and glycosides. These compounds represent those inferred from genome annotations, rather than the seed

728 compounds themselves. In panel (B), the intensity of the color indicates the average
729 log2 RPKM of the encoding gene cluster. For compounds acted upon by multiple gene
730 clusters, the percentile of the most highly-expressed cluster was chosen.
731

732 *Figure 5*
733

734 Transporters that are actively expressed by members of the acI lineage, as
735 inferred from consensus annotations of genes associated with transport reactions
736 present in metabolic network reconstructions. The intensity of the color indicates the
737 average log2 RPKM of the encoding gene cluster. For multi-subunit transporters, the
738 RPKM of the substrate-binding subunit was chosen.
739

740 *Supplementary Figure 1*
741

742 Converting an unannotated genome to a metabolic network graph, for a
743 simplified genome containing only glycolysis. **(A)** Microbial contigs are annotated using
744 KBase, and a metabolic network reconstruction is built from the annotations. The
745 reconstruction provides links between protein-encoding genes in the genome and the
746 enzymatic reactions catalyzed by those proteins. **(B)** The metabolic network
747 reconstruction represents metabolism as a hypergraph, in which metabolites are
748 represented as nodes and reactions as hyperedges. In this representation, an edge can
749 connect more than two nodes. For example, a single hyperedge (denoted by a heavy
750 black line) connects the metabolites glucose and ATP to glucose-6P, ADP, and Pi. For

clarity, protons are not shown. **(C)** However, the algorithm used by the seed set framework requires metabolism to be represented as a metabolic network graph, in which an edge can connect only two nodes. In this representation, a reaction is represented by a set of edges connecting all substrates to all products. For example, the heavy hyperedge in (B) is now denoted by six separate edges connecting glucose to ADP, glucose to Pi, glucose to glucose-6P, ATP to ADP, ATP to Pi, and ATP to glucose-6P (again denoted by heavy black lines). Of these, only one (glucose to glucose-6P) is biologically meaningful. The dotted line surrounds the currency metabolites. **(D)** The metabolic network graph is then pruned, a process which removes all currency metabolites and any edges in which those metabolites participate. Of the six heavy edges in (C), only the biologically meaningful one is retained, connecting glucose to glucose-6P (again denoted by a heavy black line). The images in (B) and (C) are modified from (Ma and Zeng, 2003).

Supplementary Figure 2

Construction of composite metabolic network graph for clade acI-C. Beginning with metabolic network graphs for genomes Actinobacterium_10 and ME00885, nodes and edges unique to ME00885 are identified (in blue). These nodes and edges are added to the Actinobacterium_10 graph, giving the composite metabolic network graph for these two genomes (Actinobacterium_10 + ME00885). Then, this graph is compared to the graph for ME03864, and nodes and edges unique to ME03864 are identified (in

773 blue). These nodes and edges are added to the Actinobacterium_10 + ME00885
774 metabolic network graph, giving the composite metabolic network graph for clade acI-C.
775

776 *Supplementary Figure 3*
777

778 Identifying seed compounds in metabolic networks, using the same metabolic
779 network as in Supplemental Figure S1. **(A)** To identify seed compounds, the metabolic
780 network graph is first decomposed into its strongly connected components (SCCs), sets
781 of nodes such that each node in the set is reachable from every other node. Here, each
782 set of circled nodes corresponds to a unique SCC. **(B)** SCC decomposition enables
783 seed sets to be identified from source components (components with no incoming
784 edges) on the condensation of the original graph. In the condensation of the original
785 graph shown here, each node corresponds to a unique SCC. This network has a single
786 seed set, SCC_1, enclosed in a dotted circle. **(C)** Seed compounds can be found from
787 the mapping between SCCs and their constituent metabolites. In this example, glucose
788 is the sole seed compound. While this particular result is probably intuitive, real
789 metabolic networks are considerably more complex. Note: The visual representations
790 shown here are intended to illustrate the metabolic network reconstruction process, and
791 are not indicative of the data structures used by our pipeline.
792

793 *Supplementary Figure 4*
794

Complete composite metabolic network graph for clade acI-C, showing disconnected components (gray) and the single largest component (green and black). Disconnected components are dropped prior to computing the network's seed sets because these groups of nodes are not connected to the bulk of the network. Within the single largest component, the giant strong component contains a substantial fraction of the compounds (green nodes), giving rise to a bow-tie structure in the metabolic network graph.

Supplementary Figure 5

Phylogenetic placement of the genomes used in this study within the acI lineage, relative to other sequenced actinobacterial genomes in the class Actinobacteria (Gao and Gupta, 2012) (Table S17). The tree was built using RAxML (Stamatakis, 2014) from a concatenated alignment of protein sequences from 37 single-copy marker genes (Darling *et al.*, 2014). The class Acidimicrobiia forms the outgroup. Vertical black bars indicate groups of genomes belonging to defined tribes/clades within the acI lineage, as determined using 16S rRNA gene sequences (for SAGs and bin FNEF8-2 bin_7 acI-B only) and a defined taxonomy (Newton *et al.*, 2011). SAGs are indicated with italic text.

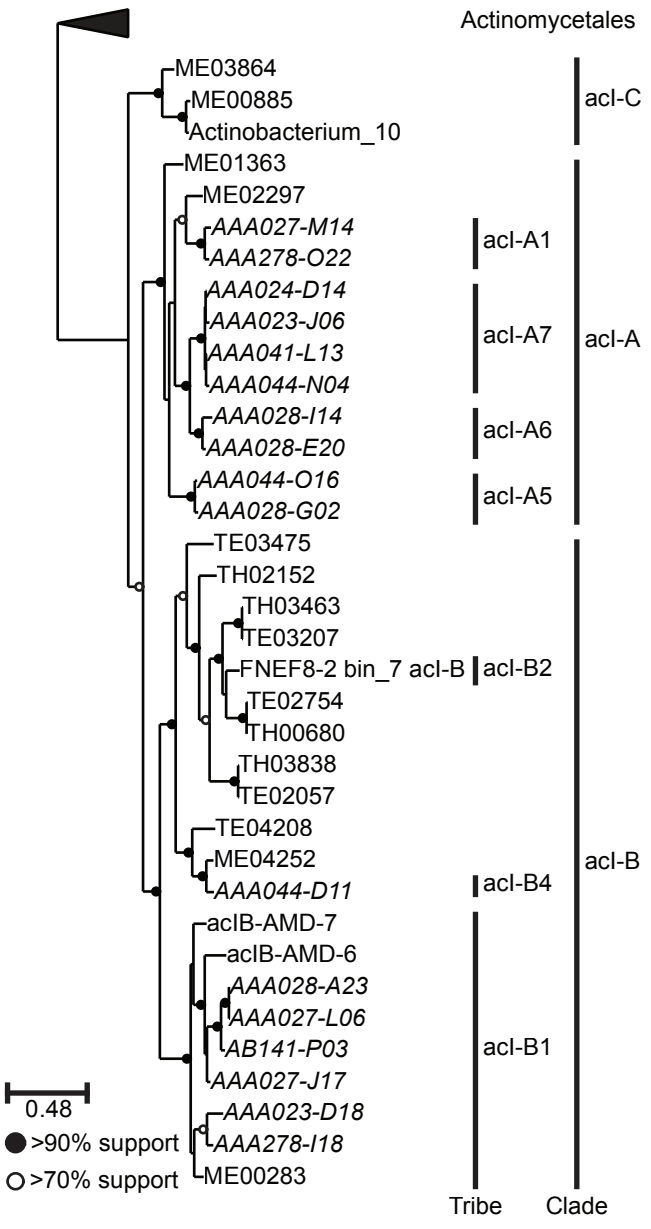
Actinomycetales
ME03864
ME00885
Actinobacterium_10
acI-C
ME01363
ME02297
AAA027-M14
AAA278-O22
acI-A1
AAA024-D14
AAA023-J06
AAA041-L13
AAA044-N04
acI-A7
acI-A
AAA028-I14
AAA028-E20
acI-A6
AAA044-O16
AAA028-G02
acI-A5
TE03475
TH02152
TH03463
TE03207
FNEF8-2 bin_7 acI-B
acI-B2
TE02754
TH00680
TH03838
TE02057
TE04208
ME04252
AAA044-D11
acI-B4
acI-B
acIB-AMD-7
acIB-AMD-6
AAA028-A23
AAA027-L06
AB141-P03
AAA027-J17
acI-B1
AAA023-D18
AAA278-I18
ME00283
0.48
>90% support
>70% support
Tribe
Clade

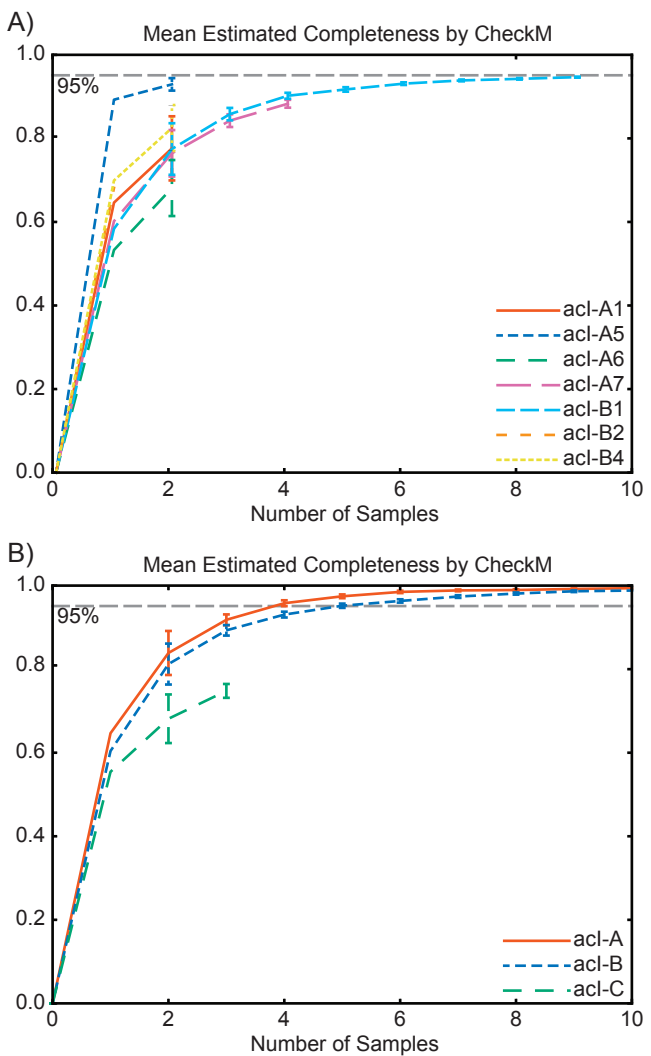
A)
Mean Estimated Completeness by CheckM
95%
1.0
0.8
0.6
0.4
0.2
0.0
0
2
4
6
8
10
Number of Samples
acI-A1
acI-A5
acI-A6
acI-A7
acI-B1
acI-B2
acI-B4
B)
Mean Estimated Completeness by CheckM
95%
1.0
0.8
0.6
0.4
0.2
0.0
0
2
4
6
8
10
Number of Samples
acI-A
acI-B
acI-C

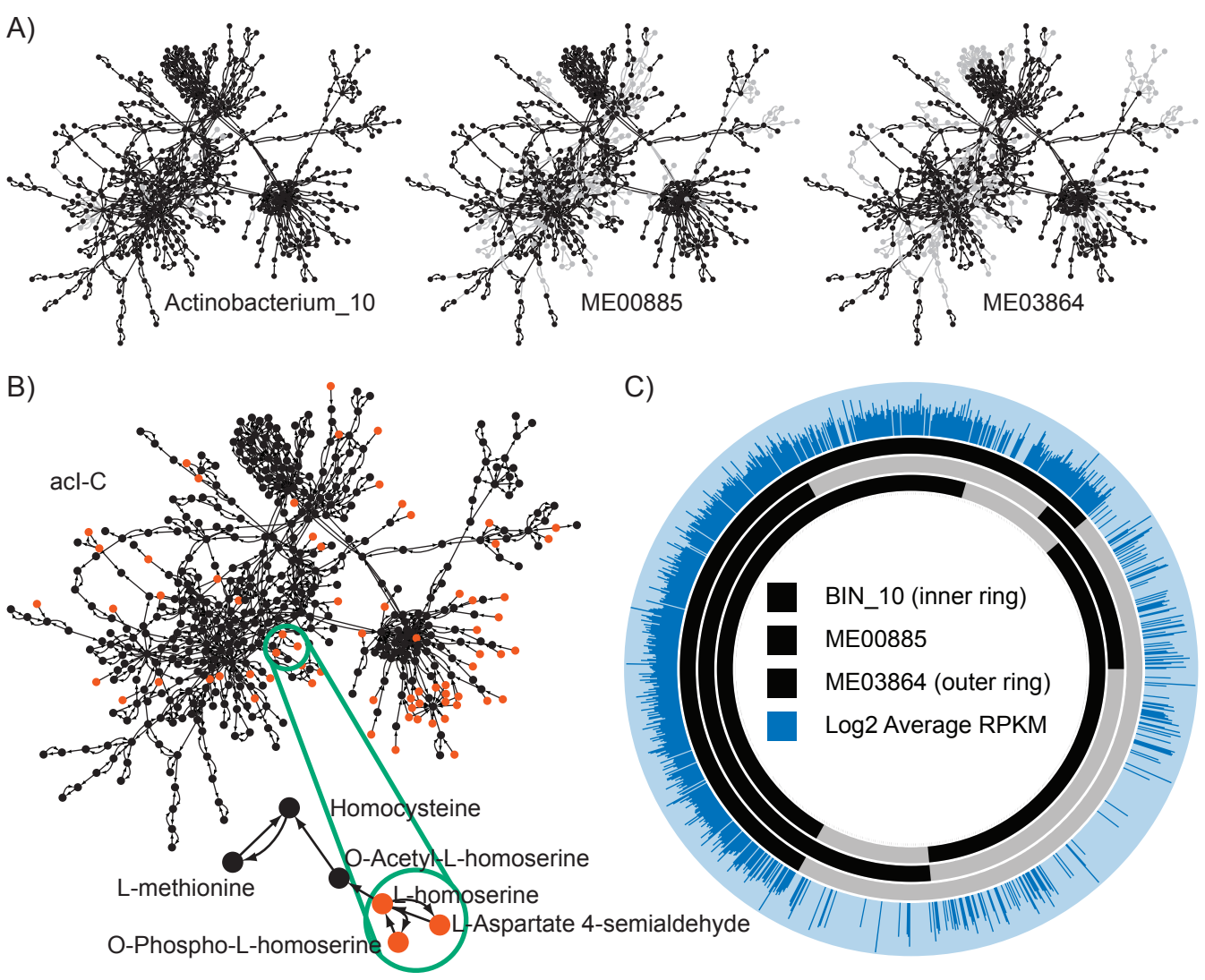
A)
Actinobacterium_10
ME00885
ME03864
B)
acl-C
Homocysteine
O-Acetyl-L-homoserine
L-methionine
L-homoserine
L-Aspartate 4-semialdehyde
O-Phospho-L-homoserine
C)
BIN_10 (inner ring)
ME00885
ME03864 (outer ring)
Log2 Average RPKM

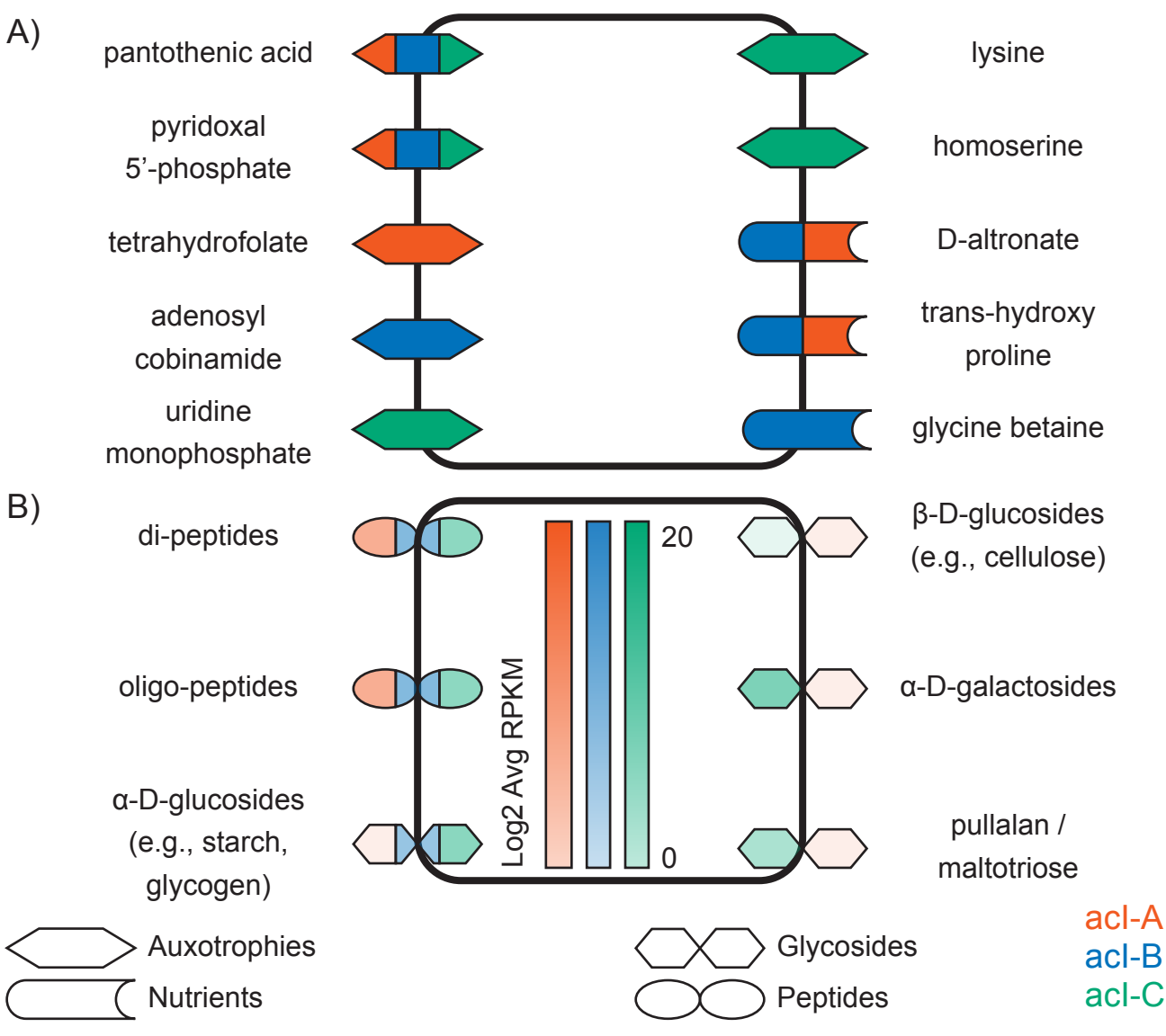
A)
pantothenic acid
pyridoxal 5'-phosphate
tetrahydrofolate
adenosyl cobinamide
uridine monophosphate
lysine
homoserine
D-altronate
trans-hydroxy proline
glycine betaine
B)
di-peptides
oligo-peptides
α-D-glucosides (e.g., starch, glycogen)
Log2 Avg RPKM
20
0
β-D-glucosides (e.g., cellulose)
α-D-galactosides
pullalan / maltotriose
Auxotrophies
Nutrients
Glycosides
Peptides
acl-A
acl-B
acl-C

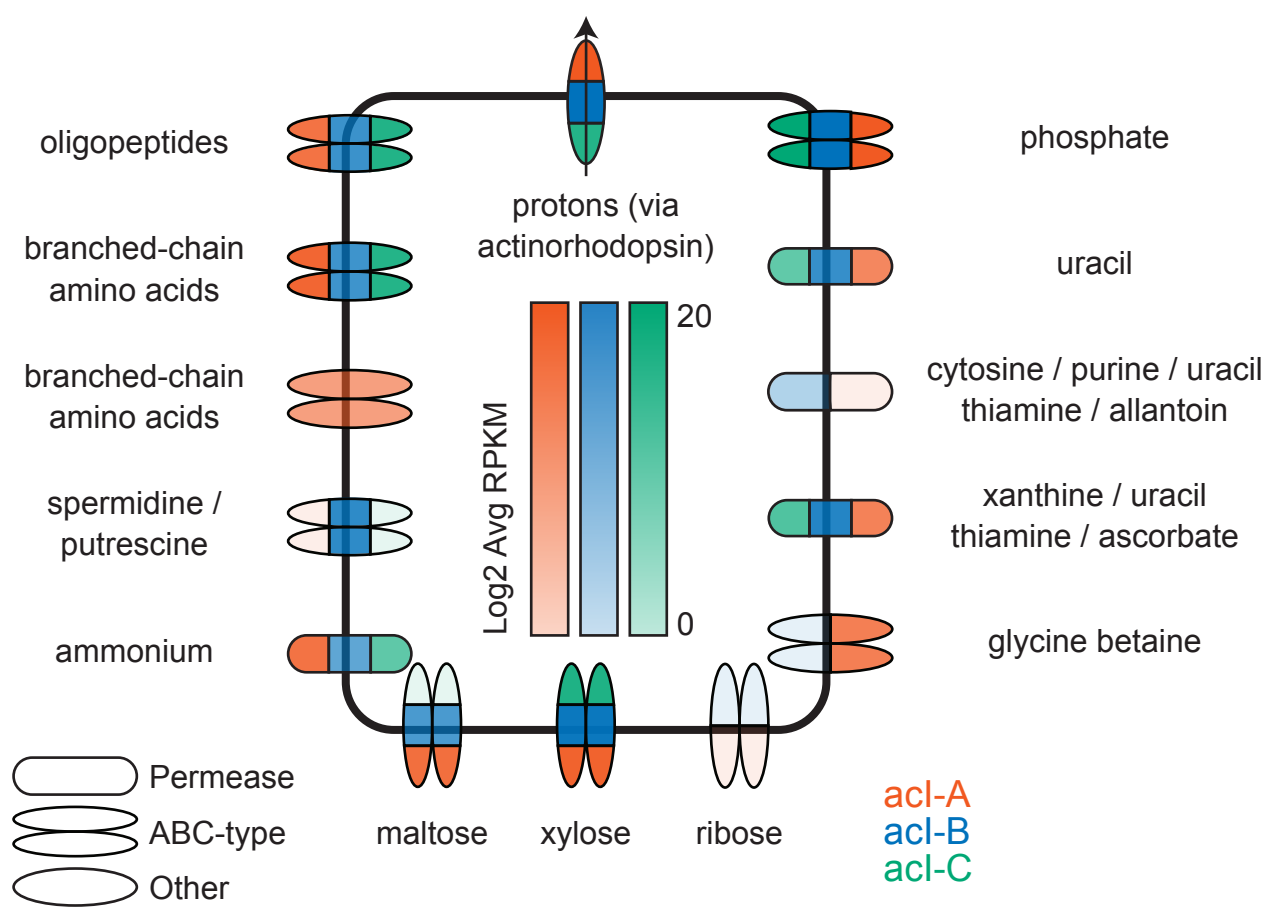
oligopeptides
branched-chain amino acids
branched-chain amino acids
spermidine / putrescine
ammonium
protons (via actinorhodopsin)
Log2 Avg RPKM
20
0
phosphate
uracil
cytosine / purine / uracil thiamine / allantoin
xanthine / uracil thiamine / ascorbate
glycine betaine
maltose
xylose
ribose
Permease
ABC-type
Other
acI-A
acI-B
acI-C

A)

>TE02754.contig.1
TCACCAAGTGAATAC
CAGCAGCACGGGCG
AGCTGAGTGATGCGA
ACGATGGACTCTTCTA
CTTCGCGAGCCGCAA
CCATCATTAGATCTGC
TAATTCATCGATGATC
ACAAGTAGGTAGGGA
TATGGTTCGAGAATTC
GCTCGCTGCCTT...

Reaction	Genes	Equation
rxn00216	TE02754.1703	glucose + ATP -> gluose-6-P + ADP + Pi
rxn00558	TE02754.1688	glucose-6-P <--> fructose-6-P
rxn00545	TE02754.2419	fructose-6-P + ATP --> fructose-1,6-P + ADP
rxn00786	TE02754.1795 OR TE02754.2367	fructose-1,6-P <--> glyceraldehyde-3-P +glycerone-P
rxn00747	TE02754.1685	glycerone-P <--> glyceraldehyde-3-P
rxn00781	TE02754.1683	glyceraldehyde-3-P + NAD + Pi <--> 1,3-P-glycerate + NADH
rxn01100	TE02754.1684	1,3-P-glycerate + ADP + Pi <--> 3-P-glycerate + ATP
rxn01106	TE02754.1899	3-P-glycerate <--> 2-P-glycerate
rxn00459	TE02754.1568 OR TE02754.1842	2-P-glycerate <--> phosphoenolpyruvate + H2O
rxn00148	TE02754.1665	phosphoenolpyruvate + ADP --> pyruvate + ATP

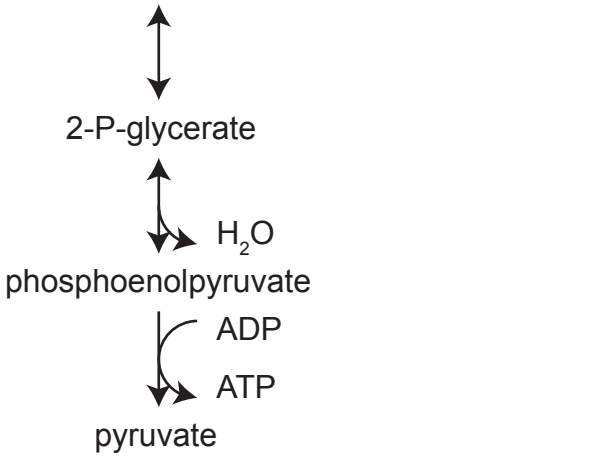

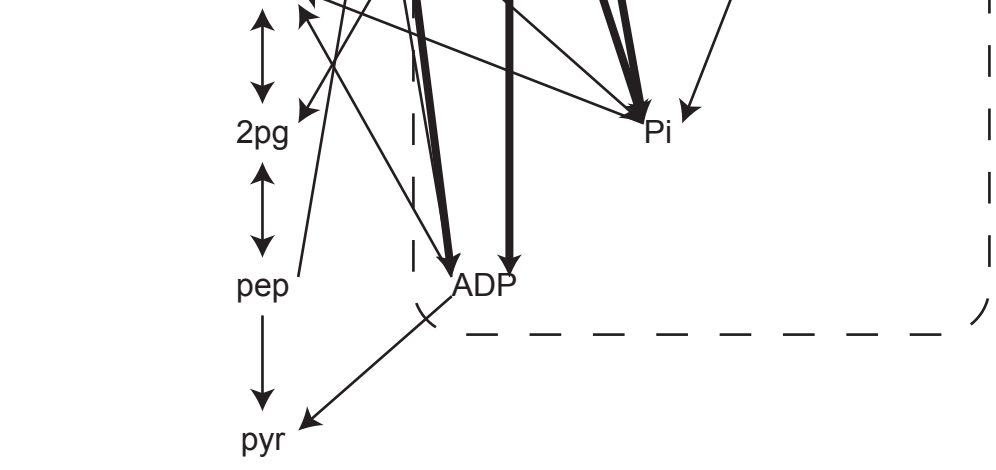

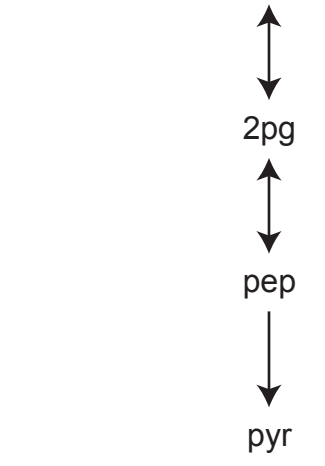

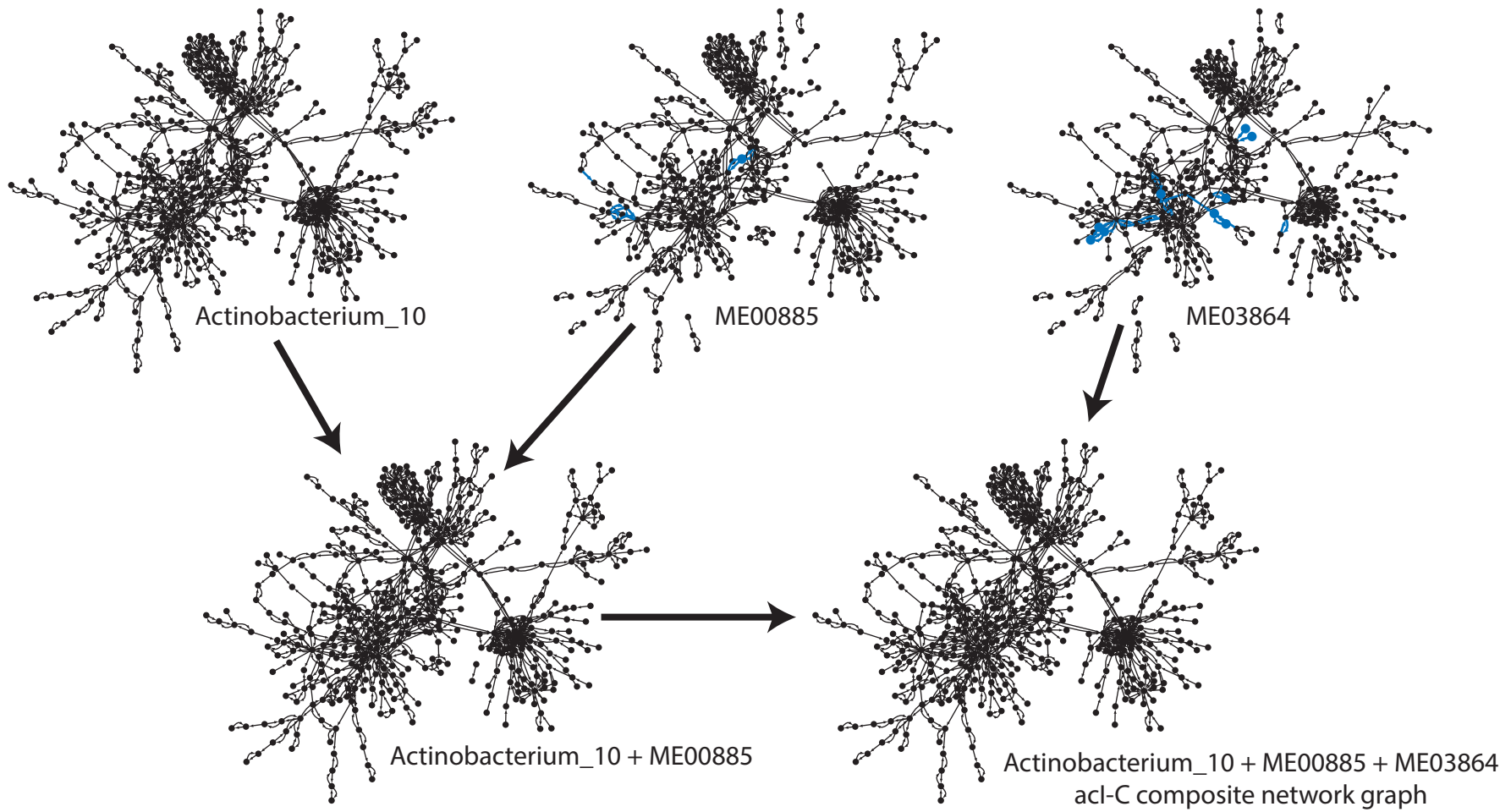
Actinobacterium_10
ME00885
ME03864
Actinobacterium_10 + ME00885
Actinobacterium_10 + ME00885 + ME03864
acl-C composite network graph

A)

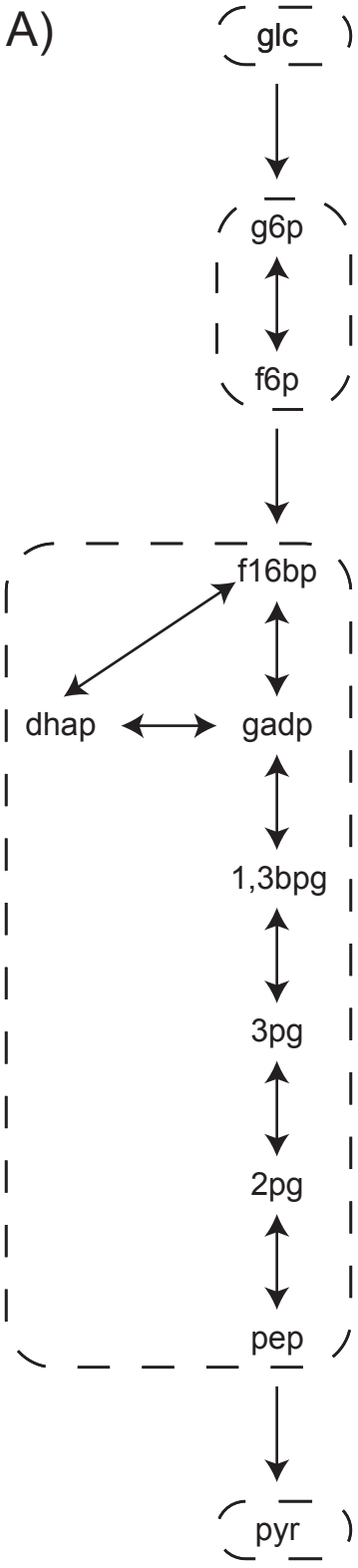

B)

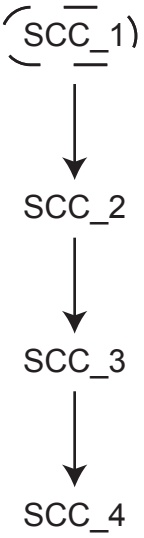

SCC	In	Out	Seed
SCC_1	0	1	Y
SCC_2	1	1	N
SCC_3	1	1	N
SCC_4	1	0	N

C)

SCC	Metabolites
SCC_1	glc
SCC_2	g6p, f6p
SCC_3	f16bp, gadp, dhap, 1,3bpg,3pg, 2pg, pep
SCC_4	pyr